Ion Mobility Studies of Electronically Excited States of Atomic Transition Metal Cations: Development of an Ion Mobility Source for Guided Ion Beam Experiments

Christopher Iceman, Chad Rue, Robert M. Moision, Barun K. Chatterjee, and P. B. Armentrout
Department of Chemistry, University of Utah, Salt Lake City, Utah, USA

The design of an ion mobility source developed to couple to a guided ion beam tandem mass spectrometer is presented. In these exploratory studies, metal ions are created continuously by electron ionization of the volatile hexacarbonyls of the three group 6 transition metals. These ions are focused into a linear hexapole ion trap, which collects the ions and then creates high intensity pulses of ions, avoiding excessive ion losses resulting from the low duty cycle of pulsed operation. The ion pulses are injected into a six-ring drift cell filled with helium where ions having different electronic configurations can separate because they have different ion mobilities. Such separation is observed for chromium ions and compares favorably with the pioneering work of Kemper and Bowers (*J. Phys. Chem.* **1991,** *95*, 5134). The results are then extended to Mo^+ and W^+, which also show efficient configuration separation. The source conditions needed for high intensities and good configuration separation are discussed in detail and suggestions for further improvements are also provided. (J Am Soc Mass Spectrom 2007, 18, 1196–1205) © 2007 American Society for Mass Spectrometry

In 1980, Johnsen and Biondi [1] made the "unexpected finding" that the mobilities in helium of ground (^4S) and metastable (^2D) states of O^+ differed. They [2] and others [3] then used this difference to conduct state-specific reactivity measurements of these systems. In 1991, Kemper and Bowers [4] discovered that such a difference in mobilities also existed for the first-row transition-metal atomic ions. Specifically, they showed that ions having different electronic configurations (and possibly specific electronic states) could be separated using ion mobility in a drift cell. They coined the term "electronic-state chromatography" to describe a time-dependent spectrum in which the various peaks correspond to different electronic configurations of the transition-metal ions. By varying the conditions used to form the ions, the authors were able to draw conclusions about the identity of the peaks, in some cases assigning not only the ground state but excited states as well. Systematically, for $Ti^+ - Zn^+$, they found that $3d^n$ configurations moved more slowly through the drift cell than $4s^1 3d^{n-1}$ configurations. This observation can be rationalized by a stronger interaction with He for the configurations having an empty 4*s* orbital [5]. Later, Taylor et al. [6] reproduced these results and extended them to second-row (Pd^+ and Ag^+) and third-row (Hf^+, Ta^+, W^+, Re^+, Ir^+, Pt^+, Au^+, and Hg^+) transition-metal ions. Although they found separations of configurations only for Pd^+, Pt^+, and Au^+, the conditions intrinsic to the glow discharge source used in these studies are likely to deactivate many excited states.

In subsequent work, Bowers and coworkers used this separation technique to examine state-specific reactions at thermal energies of Co^+ with C_3H_8, CH_3I, and rare gases [7–10], as well as Fe^+ with C_3H_8 [8], and Ni^+ and Cr^+ with rare gases [10]. Likewise, Taylor et al. adopted this technique to study the state-specific reactions of Cu^+ with CH_3Cl, CH_3Br, CH_2ClF, $CHClF_2$ and $CClF_3$ [11, 12] and Au^+ with CH_3Br [11]. One potential difficulty with this approach is that the reactions and separation are both conducted in the drift cell, such that quenching processes by the reactant molecule and other secondary effects may influence the state-specific reactivity observed.

Other approaches to examining electronic state-specific reactions of atomic transition-metal ions have also been developed. Probably the best source of pure state-specific transition-metal ions is that of resonance enhanced multi-photon ionization (REMPI) [13], which allows formation of specific electronic state and even specific spin-orbit (*J*) levels. This work requires detailed spectroscopic investigations to work out the appropriate laser excitation scheme to produce pure states. Thus,

This article honors David E. Clemmer, a very deserving recipient of the 2006 Biemann Medal.

Address reprint requests to Professor Peter B. Armentrout, Department of Chemistry, University of Utah, 315 S 1400 E Rm. 2020, Salt Lake City, UT 84112, USA. E-mail: armentrout@chem.utah.edu

1044-0305/07/$32.00
doi:10.1016/j.jasms.2007.02.012

Published online March 1, 2007
Received November 14, 2006
Revised February 16, 2007
Accepted February 16, 2007

its application has been limited to the study of V^+ with C_2H_6, C_3H_8, and C_2H_4 [13] and Fe^+ with C_3H_8 and C_4H_{10} [14]. The most extensive transition-metal ion state-specific work has arisen from our group [5, 15–30] (including several studies by Clemmer [22–24]). Using multiple ion sources to create different distributions of electronic states, the reactivity of ground and excited states of Ti^+ – Cu^+ have all been examined with a number of different neutral molecules. In contrast to the techniques mentioned above, the guided ion beam tandem mass spectrometer (GIBMS) used in these studies allows the reactions to be studied over extended ranges of kinetic energies, such that endothermic processes can be observed. One difficulty with these studies is that the characterization of the excited states relies on reactivity differences observed, specifically by quantitatively measuring threshold differences in the endothermic processes observed for different states. In many cases, because the absolute population of each state is convoluted with its relative reactivity, it is impossible to characterize how much excited state is present and, therefore, to extract absolute reaction cross sections or reaction rate constants for anything but ground state ions. Furthermore, this method is reliable when the electronic states are well separated, such as those for the first-row transition-metal ions, but cannot be applied confidently for many heavier elements where the states lie much closer together or overlap, as occurs when spin-orbit coupling becomes more important, i.e., especially for third-row transition-metal ions [31]. These various limitations have meant that very few state-specific studies have been performed for second- and third-row transition-metal ions either in our laboratories [32, 33] or others [6].

To overcome these limitations, we have developed an ion mobility source that builds on the previous studies of Biondi and Johnsen and especially Kemper and Bowers, as well as utilizing innovations introduced by Clemmer [34, 35]. By separating electronic configurations using ion mobility and controlling the energy available during the ionization process, it should be possible to select individual states for further study. The source described below has been designed to mate with our current GIBMS so that state-specific reactions over a wide range of kinetic energies can be pursued. In this paper, we offer a detailed description of the source, its characterization using Cr^+, previously studied by Kemper and Bowers, and the extension to the second- and third-row congeners, Mo^+ and W^+.

Experimental

Ion Mobility

In general, all drift studies are governed by the following equation:

$$v = KE \quad (1)$$

where v represents the velocity of the ions as they move through a bath gas under an electric field gradient E. K represents the intrinsic mobility constant of a specific ion for the conditions under which the ions are drifted and depends on temperature, pressure, mass, charge, and the interaction cross section between the ions and the bath gas. Thus, ions that are drifted under identical conditions but have dissimilar interaction cross sections will have different velocities as they move through the drift cell. This basic principle allows for a pulsed source of ions having the same mass and charge but different interaction potentials with the bath gas to be separated in time and evolve an arrival time distribution (ATD).

Ion Source

The specific details of the new source are shown in Figure 1. For the present work, ions are created by an electron ionization (EI) source, focused into a linear hexapole ion trap, pulsed into the drift cell, and then refocused by a series of ion optics for analysis in a test stand containing a quadrupole mass filter and Channeltron ion detector (Lancaster, PA). The ions of interest for the present study are the group 6 transition elements, chromium, molybdenum, and tungsten. These three elements all have stable metal hexacarbonyls that have a high vapor pressure and are easily available, and therefore amenable to EI. The metal-carbonyl vapors are leaked into the source via a Granville-Phillips leak valve (Chelmsford, PA) and ionized by electrons produced by a resistively heated tungsten filament. The electron energy can be varied from the appearance energy of the metal ion (~15 to 20 V) [36, 37] up to 100 V. The source produces generous amounts of atomic metal ions of all three metals.

Hexapole Ion Trap

In the first configuration of our ion mobility source [38], a Paul geometry quadrupole ion trap [39] was used, however, ion intensities were below those needed for

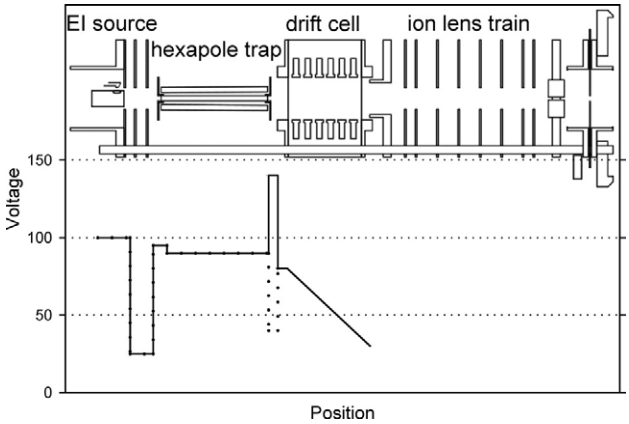

Figure 1. Configuration of the current chromatography apparatus (upper half). The lower half represents a typical set of voltage potentials used on the source as described in the text. The dotted line shows the extraction pulse used to extract ions from the trap.

use on the GIBMS largely because of the limited trapping volume of such a configuration. In addition, operation of this trapping configuration proved to be unreliable because of electronics difficulties. The duty cycle of the new source was optimized by including a linear radio frequency (rf) ion trap instead. We considered the use of a rf ring trap or ion funnel trap [40], however, the multipole trap is nicely suited for tight spatial confinement of light ions, which facilities their injection into the small orifice of the drift cell. The design of the trap builds on previous work of Clemmer and coworkers [34, 35], who found drastically increased ion intensities compared with using a Paul type quadrupole ion trap for injection into a drift cell. We believe this is largely because of the much larger trapping volume available in a linear trap coupled with better alignment with the drift cell. The linear hexapole ion trap used here was developed from versions built to thermalize ions produced by electrospray ionization [41]. This trap accumulates ions from the source continuously, thereby reducing intensity losses associated with the pulsed drift cell experiment. In addition, the use of a hexapole trap, which has an average trapping field with a radial dependence of r^{-4}, radially confines the ions and collects them along the axis of the device. This provides much better injection of the ions into the small drift cell orifice than regular ion lenses.

In our trap, the hexapole rods are 2.486 in. long and composed of 0.125 in. diameter centerless ground stainless steel held in place by Torlon rod holders (Alpharetta, GA). The hexapole rods are capped on both ends by 0.020 in. thick brass plates with a 0.125 in. orifice and a 0.039 in. gap between the plates and the end of the rods. Each brass plate includes a 0.125 in. long cylinder that extends into the rods such that ions do not feel the fringing fields associated with the ends of the rods as they are injected or extracted from the trap. The entire trap is surrounded by a temperature variable cylindrical shroud such that the trap can be pressurized to maintain ~20 mTorr of helium. Generally, helium from the drift cell is present at a pressure of about 10 mTorr and can be augmented by gas introduced through a leak valve line welded to the shroud. One interesting design feature of the trap is that the rods at the exit end of the trap have a larger bolt circle than at the entrance end. Presently, the radii from the center to the internal rod edges, r_0, are 0.1095 in. and 0.125 in. at the entrance and exit ends, respectively, making the taper only 0.38°. This provides a greater trapping volume at the exit end of the trap such that more ions collect here, enhancing the intensity of the ion pulse.

The rods are operated by home built electronics that supply a 5 MHz radio frequency signal with a maximum peak to peak output of 600 $V_{p\text{-}p}$. As shown in Figure 1, the EI source is usually held at +100 V relative to ground. An extractor lens, typically held 80 V below the source, focuses the ions from the source into the trap. The entrance plate of the hexapole trap is typically held at 5 V above the DC bias on the hexapole rods so that ions are decelerated as they are injected into the center of the hexapole trap. The DC bias on the hexapole rods is held 10 to 20 V below the source voltage to inject the ions into the hexapole ion trap, where they are rapidly thermalized by collisions with helium. During normal operation, the exit lens is held +50 V above the DC bias on the rods to keep the ions in the trap. The decelerated ions are pulsed out of the trap by capacitively coupling a −75 to −100 V extraction pulse to the exit lens, Figure 1. Effective ion pulses could be created with an extraction pulse as small as 5 V below the rods, but the most intense pulses were obtained found at 25 to 50 V below the rod DC bias. The pulse applied to the exit lens has a typical duration of 5 to 30 μs and is usually operated at a frequency of 4 kHz.

Drift Cell

Once the ions are pulsed from the ion trap they enter the drift cell, which is located 0.411 in. away with no focusing lenses in between. The general function of drift cells is well described elsewhere [42]. Our version is largely modeled after that of Kemper and Bowers [43]. Internal to the cell are six 0.188 in. thick plates with internal diameters of 1.000 in. isolated by ceramic spacers. The total cell length is 1.715 in. The cell plates and entrance/exit orifices are electrically connected with high vacuum resistors to provide the DC gradient needed to move ions from the entrance to the exit. The voltage drop across the cell can vary from 10 to 100 V depending on whether quantitative mobility studies, which require low field conditions or throughput that is better at high fields, is of primary concern. The cell is constructed entirely of copper to allow for efficient thermal regulation. The cell is usually kept near 125 K, as this provides maximum resolution of the drifted ions and aids in ion transmission (see studies below). Temperature regulation is achieved by flowing nitrogen, cooled by passing through a liquid nitrogen bath, through copper coils wrapping the cell and varying the flow rates to achieve different ultimate temperatures.

Drift cells must operate at high pressures, 0.1 to 5 torr depending on the length, to have enough collisions of the ions with the helium bath gas to cause separation. In a high vacuum system, this requires the use of small apertures, although larger apertures can be used with better pumping [44, 45]. In our current pumping configuration, provided by a single Edwards Diffstak 250 diffusion pump (West Sussex, UK), the largest apertures possible are 0.040 in. in diameter, and this configuration allows pressures of helium up to about 2 torr in the cell. If the aperture size is decreased to 0.020 in. in diameter, the pressure can increase up to about 10 torr of helium but the intensity of transmitted ions would be expected to decrease by a factor of at least eight. For an exit aperture of 0.020 in. and an entrance aperture of 0.040 in., the signal should decrease by a factor of four. The use of the smaller apertures was investigated to

further increase the pressures in the drift cell, which facilitate quantitative low-field mobility measurements. Such measurements [42] will be valuable as the mobilities of most second-row transition-metal ions have not been measured, and only those for the ground states of most third-row transition-metal ions are available [6]. However, for chemical studies using the GIBMS, maximum ion throughput combined with good separation is the primary requirement. Thus, our current configuration uses the large apertures and large drift voltages to help to minimize the loss of ions as they drift through the bath gas while still achieving separation of electronic configurations. For reasons explained below, some throughput can be sacrificed to provide a more accurate description of the arrival time distributions needed to resolve particular electronic states in the GIBMS experiments. Interestingly, even though these conditions generally exceed the low field region (<2 V/(cm torr) [42], quantitative mobility measurements can still be made, as described further below.

Ion Detection

A simple cylindrical lens train extracts the ions from the drift cell. The ions are focused by an Einzel lens followed by a set of deflectors through a 0.125 in. aperture that limits the gas load into the test stand chamber (pumped by an Edwards Diffstak 160) containing the quadrupole mass filter and detector. Because of the high-pressure in the drift cell, the kinetic energies of the ions exiting the cell are well defined, which means that focusing them is straightforward. Data acquisition is accomplished using a multichannel scaler. The scaler permits ions to be counted in bins as small as 5 ns allowing a high-resolution recording of the ATD.

As presently designed, the ion mobility source will couple to one of our laboratories guided ion beam tandem mass spectrometers (GIBMS). Details of this GIBMS instrument have been outlined previously [46, 47]. In this configuration, ions exiting the drift cell will enter the first focusing region, FS1, of the GIBMS, and then will be mass analyzed in a magnetic sector. Thus, ion pulses exiting the drift cell will be mass selected to remove unwanted ions, and then allowed to react in the octopole ion guide with all products and reactants efficiently collected and analyzed by a quadrupole mass filter and counted by a Daly type detector. Because of the high pressures used in the drift cell, it is notable that this source will provide thermalized ions in studies involving molecular species.

Results and Discussion

Experimental Conditions for Separation: Pulse Conditions

The linear hexapole ion trap allows ions to be continuously accumulated and then efficiently pulsed into the drift cell. Extensive variations of the trapping time, pulse length, and injection/extraction conditions of the trap were examined to find conditions providing maximum intensity, such that losses of ions are minimized. The intensity gain associated with the pulsed operation is difficult to measure precisely because focusing conditions for operation with and without trapping differ greatly. Nonetheless, our measurements indicate that signal improvements over pulsed operation are significant, at least an order of magnitude, compared with operation without a trap.

Pulse intensities were observed to increase with pulse length from 1 to 30 μs and then decline. The decrease at longer pulse lengths is presumably because the ion population in the trap is being depleted. Ultimately, the pulse length for the drift experiments is limited primarily to optimize the resolution of separated configurations in the ATDs. Good separation can be achieved with pulse lengths up to ~30 μs, above which separation between the observed peaks begins to be difficult. To ensure that separation between electronic configurations is not limited by the pulse length, normal operation of the source uses 3 to 5 μs pulses, which retains intensities high enough to complete experiments on the GIBMS. For such an input pulse, the pulse width of the ions extracted from the drift cell typically measures about 30 μs FWHM, and each pulse can contain as many as 1000 ions (an effective count rate of $>3 \times 10^7$ s^{-1}). At such high count rates, the ion intensity is sufficiently high that individual ion signals pile up and individual ions are no longer accurately counted. Figure 2a illustrates this effect for normalized pulses of Mo^+ ions obtained at a pulse rate of 2 kHz. The more Gaussian peak was taken at low ion intensity where individual ions are counted accurately, whereas the second peak shows the distortions that occur at very high ion intensities (absolute magnitude approximately four times that of the other peak). Space charge effects may also influence the width of the broader peak in this plot.

Under typical operating conditions, the drifted pulses usually broaden from the 3 to 5 μs starting pulse to about 30 μs although wider peaks, up to around 100 μs, are not uncommon for pulses that contain ions with different mobilities under drift conditions that result in long drift times. This limits the pulsing repetition rate to below 10 kHz to limit overlap of drifted peaks. Current operation of the source samples frequencies from 1 to 10 kHz, with the most intense pulses arising from slower rates and the most ions collected at faster rates. At slower rates, we assume the continuous supply of ions is filling the trap to capacity, resulting in pulses that are very intense but with some losses. In our experiments, there seemed to be no obvious interference between drifted ion pulses even when more than one ion packet was in the drift cell at one time. Figure 2b displays several pulses of W^+ ions collected at the highest frequency possible without risking overlap of the pulses (12.5 kHz). This figure shows that the shot-

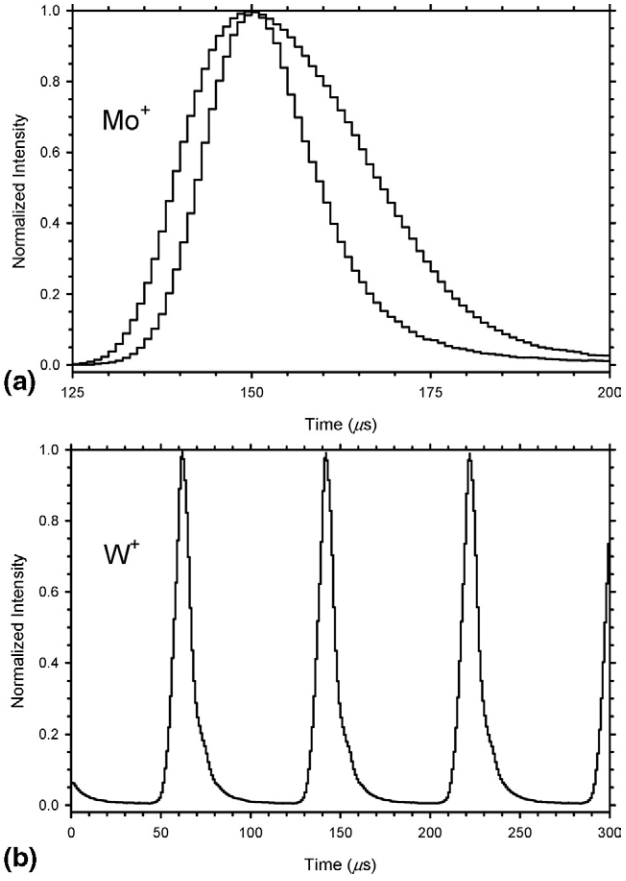

Figure 2. (**a**) Illustrates the effect of ion intensity on the pulse shape for the example of Mo^+ ions drifted in the current apparatus. The original pulse is 5 μs long. The upper curve shows a pulse having an absolute intensity about four times that of the lower, more Gaussian curve. (Conditions: Ee = 40 V, T = 200 K, P = 1.6 torr, drift field = 6 V cm^{-1}). (**b**) Depicts multiple pulses of W^+ ions drifted in a room-temperature buffer gas at a pulse frequency of 12.5 MHz. The voltage gradient across the cell is higher than normal to shorten the drift time and time spread of the ions. (Conditions: Ee = 45 V, T = 298 K, P = ~1 torr, drift field = 17 V cm^{-1}).

to-shot reproducibility of the pulses is excellent. Nevertheless, lower pulse frequencies are typically used to avoid the possibility of any overlap between subsequent ion pulses.

Figure 2b also illustrates that the peak shapes can sometimes be asymmetrical, a condition especially prominent for W^+. Some peak asymmetry is expected theoretically [42], because slower ions have more time to diffuse. Some of the tailing may be a result of the pulsing where ions at the end of the pulse will be accelerated by the return of the pulsing lens to the more positive trapping potential. Such asymmetry has been observed previously for all third-row transition-metal ions (including W^+) studied by Taylor et al. [6]. They discuss the phenomenon extensively and note that the tails correlate with the observation of other species (metal oxides or metal hydrates), which have lower mobilities. Unfortunately, the mass range of the test stand quadrupole does not permit these species to be mass analyzed, however, measurements on the GIBMS instrument indicate populations of these species to be ~7% of the W^+ beam. It is also possible that the tail could correspond to excited states, see Figure 5 below.

Experimental Conditions for Separation: Temperature Conditions

Variations in temperature of the drift cell were studied extensively. Mobilities of the transition metals depend on the temperature of the bath gas, and temperature has a direct effect on the resolution of the ATD. This is shown in eq 2,

$$resolution = (qV/8k_BT)^{1/2} \quad (2)$$

where q is the charge on the ion, V is the drift voltage, k_B is Boltzmann's constant, and T is the drift cell temperature [4]. Thus, lowering the temperature of the drift cell will reduce the diffusion of the ions, leading to better separation. Figure 3 directly illustrates the effects of temperature on the mobility of Cr^+ ions. At temperatures of 175 K or higher, the ion pulses do not adequately resolve the different electronic configurations at the cell pressure used (about 1 torr). At 135 K, the drift cell begins to produce two distinct peaks and this resolution increases until about 115 K, and then plateaus or decreases slightly at lower temperatures. It can be seen that the drift times increase as the drift cell temperatures decrease. Average drift times of the more intense peak increase from 160 μs for the 175 K plot to 225 μs for the 90 K plot. The plateau in resolution at temperatures lower than 115 K has been explained by Kemper and Bowers [4]. They point out that ion mobilities at low temperatures converge to a common value that depends only on the long-range ion-induced dipole potential, such that separation can no longer be achieved.

These studies also show that the highest intensity of

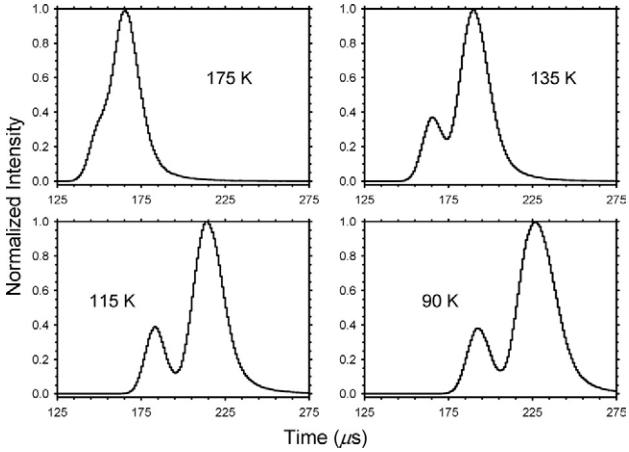

Figure 3. The temperature dependence of the resolution of Mo^+ ion configurations. (Conditions: Ee = 40 V, T as indicated, P = 1.4 to 1.6 torr, drift field = 6 V cm^{-1}).

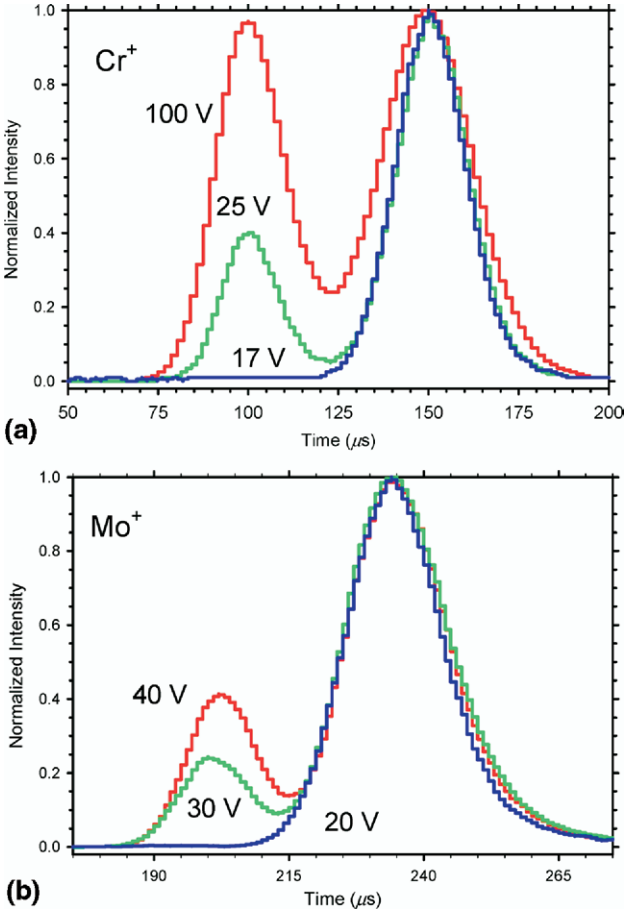

Figure 4. The dependence of the arrival time distributions on electron energy for Cr+ (**a**), conditions: Ee as shown, T = 155 K, P = 1.4 torr, drift field = 7 V cm-1) and Mo+ (**b**), conditions: Ee as shown, T = 95 K, P = 1.4 torr, drift field = 6 V cm-1).

ions per pulse is achieved at lower temperatures. Although this is not obvious in the normalized plots in Figure 3, intensities increase by 2 to 5 times from room temperature to the 115 K temperature. Lowering the temperature reduces the radial diffusion of the ions as they are pulled through the cell, thereby allowing a greater number of ions to reach the exit orifice. Typical operating temperatures vary from 200 to 100 K depending on the resolution needed to adequately separate the transition-metal configurations.

Identification of States: Dependence on Electron Energy

Variations in the electron energy (Ee) of the electron ionization source were performed to aid in identifying the ground and excited-state configurations of the transition-metal ions. As shown in Figure 4, at the lowest Ee, 17 and 20 V for Cr^+ and Mo^+, respectively, which is just above the appearance energy for production of the bare metal ions [36, 37], there is only one peak in the ATD spectrum for both metal ions. This peak must correspond to the ^6S (s^0d^5 ground state of both ions [31]. As the Ee is increased to 20 to 30 V, another peak at lower drift times appears for both metal ions with a relative magnitude that increases with increasing Ee. This identifies the higher mobility, or lower drift time peak, as corresponding to an excited-state configuration of these metal ions, specifically s^1d^4, for which a ^6D state is the lowest-lying state [31]. In our studies, the peak corresponding to the ground state is generally larger than that of the excited-state configuration, although at the largest Ees, the excited-state configuration for Cr^+ can have a comparable intensity, Figure 4.

Similar studies of varying the Ee were conducted for the case of tungsten ion. Initial attempts using a number of experimental conditions resulted in the observation of only one peak in our drift studies. This is consistent with the results of Taylor et al. who used a glow discharge metal ion source [6]. More recent studies have produced the results shown in Figure 5. At low Ee (18 V), only a single peak is observed, thereby identifying this as the ^6D ($6s^15d^4$) ground state of W^+. As the Ee is increased, a new peak at *longer* drift times is observed and becomes dominant at the highest Ee values. Clearly, this peak corresponds to excited electronic states having a $5d^5$ electronic configuration, which includes the ^6S first excited-state. Note that just as for the first and second-row congeners, states having s^1d^4 configurations appear at shorter times than those having d^5 configurations, although now the ground state has switched configurations.

Identification of States: Mobility Measurements

Another means of verifying the identity of the electronic states is to measure their mobilities. For these experiments, pulse widths were kept ≤1 μs, the temperature at 120 K, and the pressure at 1.25 torr. Arrival times were measured as a function of the applied drift field (5 to 30 V), corresponding to E/P values between 0.9 and

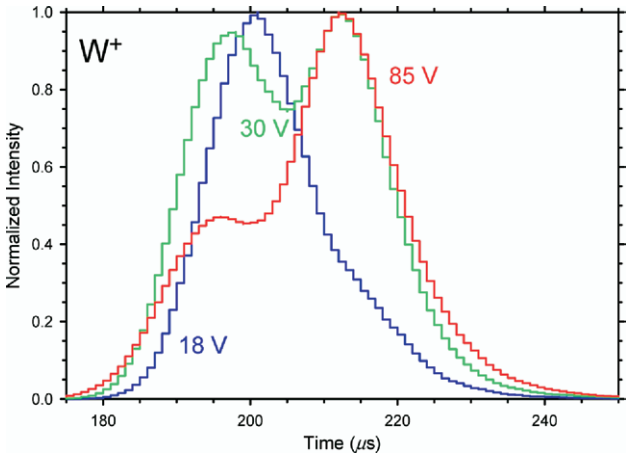

Figure 5. The dependence of the arrival time distributions on electron energy for W^+ at Ee = 18 (blue line), 30 (green line), and 85 (red line) eV. (Conditions: Ee as shown, T = 120 K, P = 1.4 torr, drift field = 7 V cm^{-1}).

Table 1. Single temperature (120 K) reduced field mobilities (in $cm^2/(V\ s)$ of group 6 and argon cations

Ion	Configuration[a]	K_0 (this work)	K_0 (literature)
Ar^+	$3s^23p^5$	20.7 ± 2.1	19.0 ± 1.5 (180 K)[b]
Cr^+	$3d^5$ (GS)	18.9 ± 1.9	18 ± 0.3 (298 K),[c] 16.4 ± 1.1 (160 K)[b]
	$4s^13d^4$	24.6 ± 2.5	23.0 ± 1.6 (160 K)[b]
Mo^+	$4d^5$ (GS)	18.5 ± 1.9	
	$5s^14d^4$	23.4 ± 2.3	
W^+	$6s^15d^4$ (GS)	22.7 ± 2.3	19.7 ± 0.9 (~195 K)[c]
	$5d^5$	20.5 ± 2.1	

[a]GS = ground state.
[b]Reference 4.
[c]Reference 6.

5.5 V/(cm torr) or E/N values of 1.1 to 6.8 Td. The higher values exceed the low field region (<2 V/(cm torr) [42], but good linearity of the plots was found in all cases, indicating no high field deviations. The resulting reduced field mobilities for all three group 6 metal ions as well as Ar^+, taken from the slope of a plot of arrival time versus 1/V [4], are reported in Table 1. Reported uncertainties are the combined uncertainties associated with the pressure and temperature measurements, the measured slope, and the effect of ion penetration into the drift cell [4]. For all values, the mobilities reported lie within the combined uncertainties of the available literature values. Observed deviations can be largely attributed to the different temperatures at which the values are measured. Values for the ground and excited states of Mo^+ are reported here for the first time. These values are similar to those of other transition-metal ion mobilities. The only other second-row transition-metal ion mobility available is for Pd^+ in its ground and first excited states. Taylor, et al. [6] measure reduced mobilities of 18.2 and 23.2 for the $4d^9$ and $5s^14d^8$ configurations of Pd^+, respectively, very similar to the values measured here for the analogous configurations of Mo^+. Finally, we note that the relative mobilities of the ground and excited states of W^+ are comparable to those for the analogous configurations of the first- and second-row congeners, helping to confirm the identity of these states.

rf Effects on Deactivation

Trapping conditions in the linear hexapole trap were thoroughly investigated to observe effects on ion intensity and separation of electronic configurations. As noted above, ions are continuously injected into the hexapole trap with around 5 V of kinetic energy, after which the ions quickly thermalize and then diffuse to the exit of the trap for extraction. Generally, the ions are subjected to 150 to 400 $V_{p\text{-}p}$ of rf voltage on the rods. It was found that higher rf voltages gave higher intensities but also exhibited lower ratios of excited-state to ground state configurations of the transition-metal ions. Figure 6a shows sequential studies of the ATDs of Mo^+ ions at different rf fields where the total ion intensity is held constant. One curve shows results for a trapping field of 350 $V_{p\text{-}p}$. As the rf field increases up to 450 $V_{p\text{-}p}$ and above while keeping the total ion intensity constant, it can be seen that the relative intensities of the two peaks change as does the resolution, indicating deactivation of the excited-state. Similar deactivation is not observed if the intensity of the ions is enhanced by increasing the electron emission current in the ion source, as shown in Figure 6b. We believe that deactivation is correlated with increased ion densities, induced by the higher trapping potentials as the rf voltage is increased. If the ion densities are sufficiently high, ion-ion collisions, which can have very long-range effects because of the 1/R distance dependence of the Coulomb potential, may induce deactivation.

Analysis of the Cr^+ ATD

To evaluate the qualitative ATDs of our drift cell to previous results, the test case of Cr^+ was used for comparison. Kemper and Bowers [4] found that the relative intensities in the ATDs of first-row transition

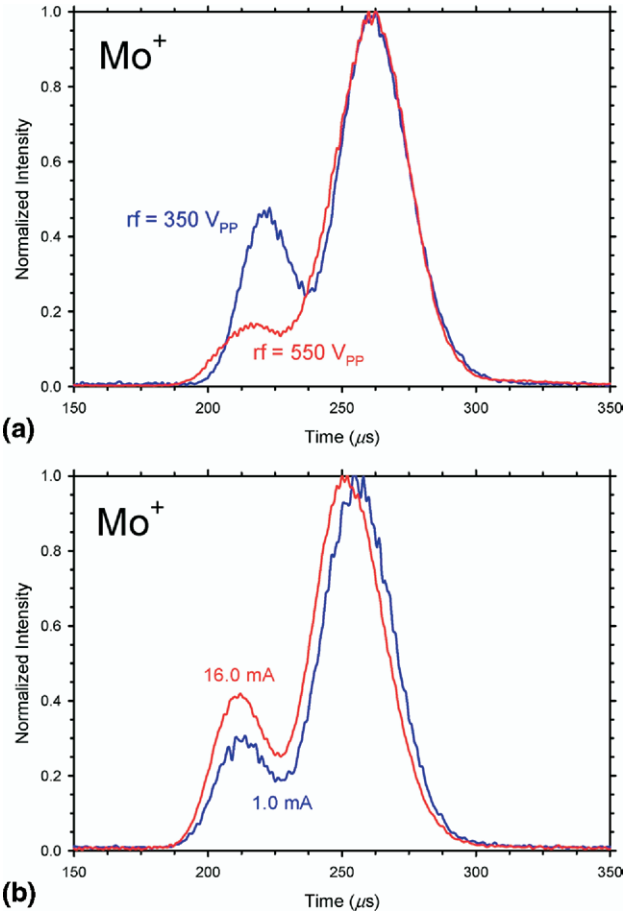

Figure 6. The dependence of the arrival time distributions on rf $V_{p\text{-}p}$ (**a**), $V_{p\text{-}p}$ = 350 V, blue line, $V_{p\text{-}p}$ = 550 V, red line) and source emission current (**b**), emsrc = 1.0 mA, blue line, emsrc = 16.0 mA, red line) for Mo^+ ions. (Conditions: Ee = 50 V, T = 120 K, Vpp = 400 V unless specified, P = 1.25 torr, drift field = 7 V cm^{-1}).

metals showed a direct dependence on the initial electron energy at the ion creation source. This dependence enabled the authors to draw conclusions as to the nature of the different peaks, label excited-state or ground state configurations, and calculate the abundance ratios of the various states. Data shown in Figure 4a qualitatively reproduces these previous results, although relative peak intensities may be skewed from effects of rf quenching in the hexapole ion trap as discussed above. Figure 7 directly compares data for Cr^+ from Kemper and Bowers [4] obtained using a CrO_2Cl_2 precursor (Fig 7a) with our data using a $Cr(CO)_6$ precursor (Fig 7b–d). Temperature conditions are similar but the higher pressures used by Kemper and Bowers lead to longer drift times and better separation.

To further quantify the results from our laboratory, we have tried to reproduce the ATDs using a fitting program. This procedure is difficult for several reasons. Although ATD peaks are generally Gaussian, small tails associated with intense pulses or harsh drift conditions can skew the peaks. As noted above, pileup of ions can also distort the normally symmetric peaks. Reproduction of peaks that are not well resolved or peaks in which deactivation is occurring can lead to multiple fits of the data that provide adequate representation of the total ATD distribution. An example of these difficulties can be seen in Figure 7. Figure 7b depicts the fitting of Cr^+ data collected at high drift field conditions with two large peaks using a simple iterative fitting function in MATLAB [48] that utilizes Gaussian peaks. It can be seen that the fit describes the peak at longer drift times very well, however, the fit of the earlier peak fails to describe its center and base accurately. Figure 7c shows a fit that focuses on reproducing only the outer portions of both peaks. The discrepancy between this fit and the data suggests that there may be a third peak in the spectrum lying between the two major features. Indeed, Kemper and Bowers [4] found a similar third peak for Cr^+ that arose at high electron energies. Figure 7d shows that addition of such a peak accurately describes the entire ATD spectrum. It should be noted that there were multiple fits of the short drift time peak that provided an adequate description of the overall ATD,

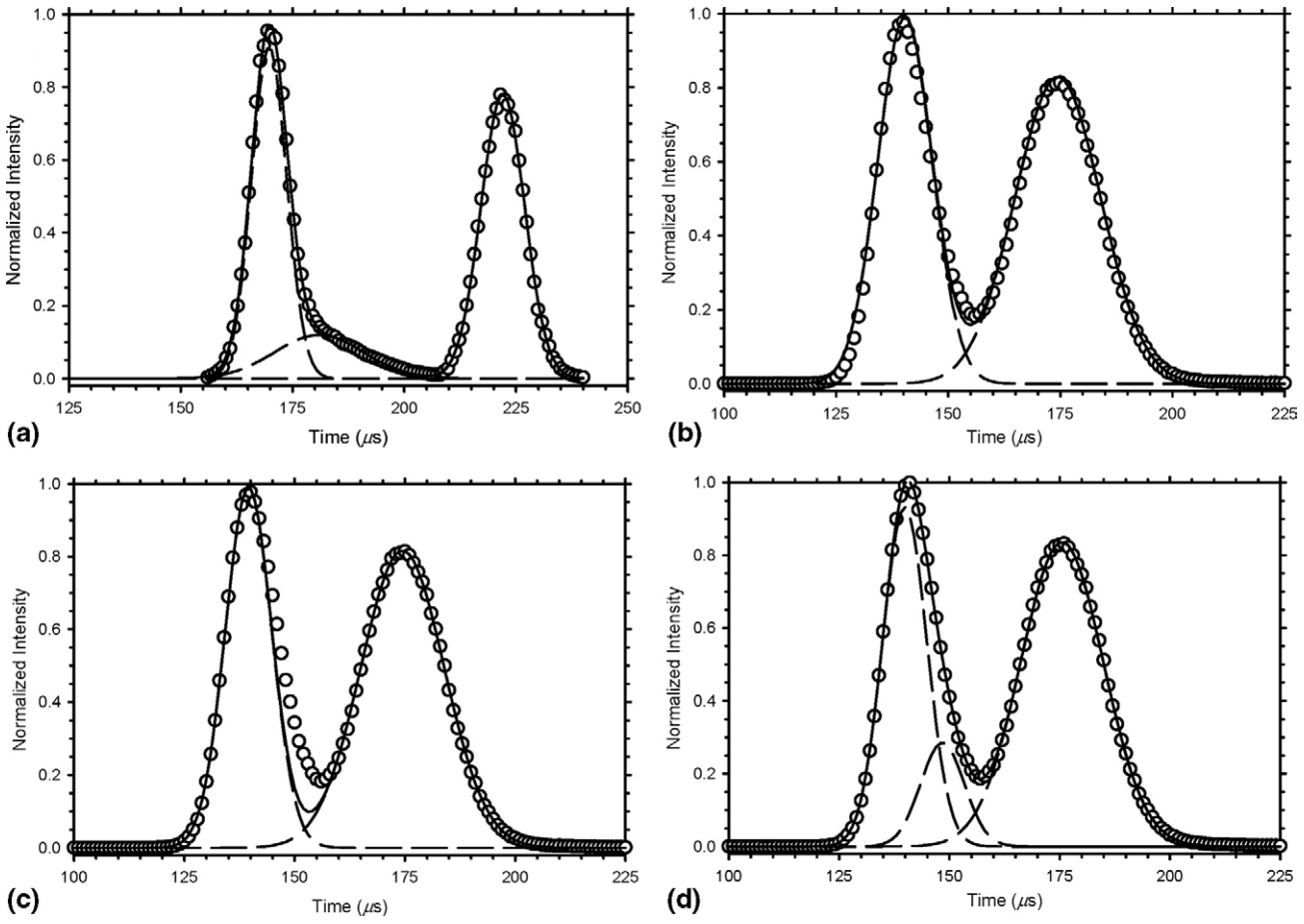

Figure 7. Analysis of Cr^+ ion arrival time distributions from Kemper and Bowers (**a**), [4] conditions: CrO_2Cl_2, Ee = 40.5 V, T = 152 K) and this study (**b**), (**c**), (**d**), conditions: $Cr(CO)_6$, Ee = 100 V, T = 155 K, P = 1.4 torr, drift field = 6 V cm^{-1}) using Gaussian peak shapes. (**b**) Shows the ATD peaks fitted iteratively in MATLAB with a two peak distribution, (**c**) shows the ATD peaks fitted with an emphasis on the outer points, and (**d**) shows a fit with 3 Gaussians.

with ratios in the intensities of the two Gaussians varying by over a factor of two.

This fitting program was also applied to the Cr^+ results (CrO_2Cl_2 precursor ionized at 40.5 eV) from Kemper and Bowers [4], and those results can be seen in Figure 7a. Here three peaks, as described by the authors, provide an adequate fit to the overall ATD, but in this analysis, the central peak of the ATD must be wider than the other two (by a factor of two). In the low field conditions used by Kemper and Bowers, the width of all peaks in the absence of deactivation should be uniform as it is only a function of voltage, charge, and temperature [4], as specified in eq 2 above. The relative widths of the peaks suggest that this middle peak may correspond to multiple peaks having $4s^13d^4$ configurations but somewhat different mobilities or that at these elevated electron energies, more highly excited states are being produced and undergoing deactivation to the ground state. Kemper and Bowers ruled out such deactivation at lower electron energies and stated that no deactivation between ground and excited states was observed at room temperature. Increased resolution of our data as well as reactions done on the GIBMS should be able to provide insight into the true states present in the ATD.

Application to GIBMS Studies

The experiments above demonstrate that the new ion mobility source has the ability to separate transition-metal ions having different electronic configurations for both first-, second-, and third-row metals. To exploit this ability in GIBMS experiments, a number of issues need to be explored to optimize the use of this source. Specifically, the source needs to provide sufficient ion intensity with good stability. Further, the pulsed operation intrinsic to separation in the drift cell may necessitate a different mode of data collection. Three possible means of determining configuration-specific reactivity can be envisioned. If the temporal separation between ion pulses is maintained during reaction in the collision cell, the collection of reaction cross sections for different configurations can be achieved simultaneously by monitoring reactant and product ion intensities as a function of time. If the separation is not maintained during reaction, then it may be necessary to gate only one configuration at a time into the reaction zone and measure their reaction cross sections independently. In this case, the temporal profiles of the reactant and product ions need not be monitored. Alternatively, the drift cell could be used to characterize the state distributions of ions under specific ionization conditions, and then the reactivity of these distributions could be studied in a continuous mode. By varying the ionization conditions to alter the state distributions, the results of such studies can be combined to yield state-specific information, similar to the methods used for previous state-specific experiments performed in our laboratory [5, 15–30]. As noted above, however, because the absolute quantities of the configurations would be characterized, absolute cross sections for ground and excited states could now be extracted from this procedure.

Typically, the examination of the reactions of atomic transition-metal ions with H_2, CH_4, and other hydrocarbons require ion beam intensities of 10^5 to 10^6 per second because the cross section for these reactions can be small, single collision conditions are needed, and a careful examination of threshold behavior requires as much intensity as possible. Ion intensities of this magnitude have been achieved on the test stand, but successful mating to the GIBMS will require careful attention to minimizing ion losses between the source and the GIBMS.

For such experiments, the source also must be stable over the course of hours, ideally in terms of intensity but primarily with regard to the separation established between ions having different configurations. As yet, it is unclear whether the ATDs can be relied upon not to deviate appreciably over the course of such an experiment. Such degradation could occur from EI filament degradation, and pressure and temperature fluctuations in the drift cell. In experiments to date, the ATDs have exhibited instabilities that alter the arrival times as well as peak intensities and relative ratios for different configurations. However, once the ion signal is optimized and the drift cell temperature equilibrated, both the ATDs and the pulse intensity have been stable for hours.

To augment the EI source currently employed to generate metal ions, laser ablation and glow discharge sources for the ion mobility source are being developed. A laser ablation source of ions would be intrinsically pulsed and would still allow variation of state distributions by varying laser power. Furthermore, such a source is much more general, no longer relying of the existence of volatile organometallic precursors, and avoids potential difficulties associated with having these precursors in the ion trapping regions, which may lead to excited-state deactivation, as discussed above.

The design of the hexapole trap and drift cell is also conducive to coupling to other types of ion sources. For instance, the electrospray ionization source presently being developed in our laboratory [41] can be mated to the present hexapole trap/drift cell chamber, allowing the possibility of separating complex biomolecules having different conformations. Measuring quantitative conformation-specific thermochemistry is an intriguing idea that can be realized with such an approach.

Acknowledgments

Funding for this project is provided by the National Science Foundation, grant CHE-0451477. The authors thank Paul Kemper for advice throughout the years in developing this source. They thank the reviewers for their substantive comments.

References

1. Johnsen, R.; Biondi, M. A. Charge Transfer Coefficients for the $O^+(^2D)$ + N_2 and $O^+(^2D)$ + O_2 Excited Ion Reactions at Thermal Energy. *J. Chem. Phys.* **1980,** *73,* 190–193.
2. Johnsen, R.; Biondi, M. A.; Hayashi, M. Mobilities of Ground-State and Metastable O^+, O_2^+, O^{2+}, and O_2^{2+} Ions in Helium and Neon. *J. Chem. Phys.* **1982,** *77,* 2545–2548.
3. Rowe, B. R.; Fahey, D. W.; Fehsenfeld, F. C.; Albritton, D. L. Rate Constants for the Reactions of Metastable O^{+*} Ions with N_2 and O_2 at Collision Energies 0.04 to 0.2 eV and the Mobilities of These Ions at 300 K. *J. Chem. Phys.* **1980,** *73,* 194–205.
4. Kemper, P. R.; Bowers, M. T. Electronic-State Chromatography: Application to First-Row Transition-Metal Ions. *J. Phys. Chem.* **1991,** *95,* 5134–5146.
5. Loh, S. K.; Fisher, E. R.; Lian, L.; Schultz, R. H.; Armentrout, P. B. State Specific Reactions of $Fe^+(^6D, ^4F)$ with O_2 and cyclo-C_2H_4O: $D^o{}_0(Fe^+\text{-}O)$ and Effects of Collisional Relaxation. *J. Phys. Chem.* **1989,** *93,* 3159–3167.
6. Taylor, W. S.; Spicer, E. M.; Barnas, D. F. Metastable Metal Ion Production in Sputtering dc Glow Discharge Plasmas: Characterization by Electronic State Chromatography. *J. Phys. Chem. A* **1999,** *103,* 643–650.
7. van Koppen, P. A. M.; Kemper, P. R.; Bowers, M. T. Reactions of State-Selected Co^+ with C_3H_8. *J. Am. Chem. Soc.* **1992,** *114,* 1083–1084.
8. van Koppen, P. A. M.; Kemper, P. R.; Bowers, M. T. Electronic State-Selected Reactivity of Transition Metal Ions: Co^+ and Fe^+ with Propane. *J. Am. Chem. Soc.* **1992,** *114,* 10941–10950.
9. van Koppen, P. A. M.; Kemper, P. R.; Bowers, M. T. Fundamental Studies of the Energetics and Dynamics of State-Selected Co^+ Reacting with CH_3I. The Co^+-CH_3 and Co^+-I Bond Energies. *J. Am. Chem. Soc.* **1993,** *115,* 5616–5623.
10. Kemper, P. R.; Hsu, M.-T.; Bowers, M. T. Transition-Metal Ion—Rare Gas Clusters: Bond Strengths and Molecular Parameters for $Co^+(He/Ne)_n$, $Ni^+(He/Ne)_n$, and $Cr^+(He/Ne/Ar)$. *J. Phys. Chem.* **1991,** *95,* 10600–10609.
11. Taylor, W. S.; May, J. C.; Lasater, A. S. Reactions of $Cu^+(^1S,^3D)$ and $Au^+(^1S,^3D)$ with CH_3Br. *J. Phys. Chem. A* **2003,** *107,* 2209–2215.
12. Taylor, W. S.; Matthews, C. C.; Parkhill, K. S. Reactions of $Cu^+(^1S, ^3D)$ with CH_3Cl, CH_2ClF, $CHClF_2$, and $CClF_3$. *J. Phys. Chem. A* **2005,** *109,* 356–365.
13. Sanders, L.; Hanton, S. D.; Weisshaar, J. C. Total Reaction Cross Sections of Electronic State-Specified Transition Metal Cations: V^+ + C_2H_6, C_3H_8, C_2H_4 at 0.2 Ev. *J. Chem. Phys.* **1990,** *92,* 3498–3518.
14. Hanton, S. D.; Noll, R. J.; Weisshaar, J. C. Electronic-State-Specific Transition Metal Cation Chemistry: $Fe^+ + C_3H_8$ and $n - C_4H_{10}$. *J. Chem. Phys.* **1992,** *96,* 5176–5190.
15. Elkind, J. L.; Armentrout, P. B. Effect of Kinetic and Electronic Energy on the Reaction of V^+ with H_2, HD, and D_2. *J. Phys. Chem.* **1985,** *89,* 5626–5636.
16. Aristov, N.; Armentrout, P. B. Reaction Mechanisms and Thermochemistry of $V^+ + C_2H_{2p}$ (P = 1, 2, 3). *J. Am. Chem. Soc.* **1986,** *108,* 1806–1819.
17. Elkind, J. L.; Armentrout, P. B. Effect of Kinetic and Electronic Energy on the Reactions of Fe^+ with H_2, HD, and D_2: State-Specific Cross Sections for $Fe^+(^6D)$ and $Fe^+(^4F)$. *J. Phys. Chem.* **1986,** *90,* 5736–5745.
18. Elkind, J. L.; Armentrout, P. B. State-Specific Reactions of Atomic Transition Metal Ions with H_2, HD, and D_2: Effects of d-Orbitals on Chemistry. *J. Phys. Chem.* **1987,** *91,* 2037–2045.
19. Schultz, R. H.; Elkind, J. L.; Armentrout, P. B. Electronic Effects in C–H and C–C Bond Activation: State-Specific Reactions of $Fe^+(^6D, ^4F)$ with Methane, Ethane, and Propane. *J. Am. Chem. Soc.* **1988,** *110,* 411–423.
20. Armentrout, P. B. Chemistry of Excited Electronic States. *Science* **1991,** *251,* 175–179.
21. Fisher, E. R.; Armentrout, P. B. Electronic Effects in C–H and C–C Bond Activation: Reactions of Excited State Cr^+ with Propane, Butane, Methylpropane, and Dimethylpropane. *J. Am. Chem. Soc.* **1992,** *114,* 2049–2055.
22. Clemmer, D. E.; Chen, Y.-M.; Khan, F. A.; Armentrout, P. B. State-Specific Reactions of $Fe^+(a^6D, a^4F)$ with D_2O and Reactions of FeO^+ with D_2. *J. Phys. Chem.* **1994,** *98,* 6522–6529.
23. Clemmer, D. E.; Chen, Y.-M.; Aristov, N.; Armentrout, P. B. Kinetic and Electronic Energy Dependence of the Reaction of V^+ with D_2O. *J. Phys. Chem.* **1994,** *98,* 7538–7544.
24. Chen, Y.-M.; Clemmer, D. E.; Armentrout, P. B. Kinetic and Electronic Energy Dependence of the Reactions of Sc^+ and Ti^+ with D_2O. *J. Phys. Chem.* **1994,** *98,* 11490–11498.
25. Kickel, B. L.; Armentrout, P. B. Guided Ion Beam Studies of the Reactions of Ti^+, V^+, and Cr^+ with Silane. Electronic State Effects, Comparison to Reactions with Methane, and M^+-SiH_x (x = 0-3) Bond Energies. *J. Am. Chem. Soc.* **1994,** *116,* 10742–10750.
26. Kickel, B. L.; Armentrout, P. B. Reactions of Fe^+, Co^+, and Ni^+ with Silane. Electronic State Effects and M^+-SiH_x (x = 0–3) Bond Energies. *J. Am. Chem. Soc.* **1995,** *117,* 764–773.
27. Kickel, B. L.; Armentrout, P. B. Guided Ion Beam Studies of the Reactions of Group 3 Metal Ions (Sc^+, Y^+, La^+, and Lu^+) with Silane. Electronic State Effects, Comparison to Reactions with Methane, and M^+-SiH_x (x = 0–3) Bond Energies. *J. Am. Chem. Soc.* **1995,** *117,* 4057–4070.
28. Rue, C.; Armentrout, P. B.; Kretzschmar, I.; Schroder, D.; Harvey, J. N.; Schwarz, H. Kinetic-Energy Dependence of Competitive Spin-Allowed and Spin-Forbidden Reactions: $V^+ + CS_2$. *J. Chem. Phys.* **1999,** *110,* 7858–7870.
29. Rodgers, M. T.; Walker, B.; Armentrout, P. B. Reactions of $Cu^+(^1S$ and $^3D)$ with O_2, CO, CO_2, NO, N_2O, and NO_2 Studied by Guided Ion Beam Mass Spectrometry. *Int. J. Mass Spectrom.* **1999**, *182/183,* 99–120.
30. Rue, C.; Armentrout, P. B.; Kretzschmar, I.; Schroder, D.; Schwarz, H. Guided Ion Beam Studies of the State-Specific Reactions of Cr^+ and Mn^+ with CS_2 and COS. *Int. J. Mass Spectrom.* **2001**, *210/211,* 283–301.
31. National Institute of Standards and Technology; NIST Atomic Spectra Database, http://physics.nist.gov/PhysRefData/ASD/levels_form.html, 2006.
32. Zhang, X.-G.; Armentrout, P. B. Activation of O_2, CO, and CO_2 by Pt^+: The Thermochemistry of PTO^+. *J. Phys. Chem. A* **2003,** *107,* 8904–8914.
33. Li, F.-X.; Armentrout, P. B. Activation of Methane by Gold Cations: Guided Ion Beam and Theoretical Studies. *J. Chem. Phys.* **2006,** *125,* 133111–133114.
34. Hoaglund, C. S.; Valentine, S. J.; Clemmer, D. E. An Ion Trap Interface for ESI-Ion Mobility Experiments. *Anal. Chem.* **1997,** *69,* 4156–4161.
35. Myung, S.; Lee, Y. J.; Moon, M. H.; Taraszka, J.; Sowell, R.; Koeniger, S.; Hilderbrand, A. E.; Valentine, S. J.; Cherbas, L.; Cherbas, P.; Kaufmann, T. C.; Miller, D. F.; Mechref, Y.; Novotny, M. V.; Ewing, M. A.; Sporleder, C. R.; Clemmer, D. E. Development of High-Sensitivity Ion Trap Ion Mobility Spectrometry Time-of-Flight Techniques: A High Throughput Nano-LC-IMS-TOF Separation of Peptides Arising from a *Drosophila* Protein Extract. *Anal. Chem.* **2003,** *75,* 5137–5145.
36. Das, P. R.; Nishimura, T.; Meisels, G. G. Fragmentation of Energy-Selected Hexacarbonylchromium Ion. *J. Phys. Chem.* **1985,** *89,* 2808–2812.
37. Michels, G. D.; Flesch, G. D.; Svec, H. J. Comparative Mass Spectrometry of the Group 6B Hexacarbonyls and Pentacarbonyl Thiocarbonyls. *Inorg. Chem.* **1980,** *19,* 479–485.
38. Rue, C. Ph.D. Thesis, University of Utah, 2000.
39. Ghosh, P. K. *Ion Traps*; Oxford University Press: New York, 1995, pp. 1–46.
40. Tang, X.; Ens, W.; Standing, K. G.; Westmore, J. B. Daughter Ion Mass Spectra from Cationized Molecules of Small Oligopeptides in a Reflecting Time-of-Flight Mass Spectrometer. *Anal. Chem.* **1988,** *60,* 1791–1799.
41. Moision, R. M.; Armentrout, P. B. The Electrospray: A New Source for Thermochemical Investigation with the Guided Ion Beam Mass Spectrometer. *J. Am. Soc. Mass Spectrom.*, unpublished.
42. McDaniel, E. W.; Mason, E. A. *The Mobility and Diffusion of Ions in Gases*; Vol. I; John Wiley and Sons: New York, 1973, pp. 1–84.
43. Kemper, P. R.; Bowers, M. T. A Hybrid Double-Focusing Mass Spectrometer High-Pressure Drift Reaction Cell to Study Thermal Energy Reactions of Mass-Selected Ions. *J. Am. Soc. Mass Spectrom.* **1990,** *1,* 197–207.
44. Lee, Y. J.; Hoaglund-Hyzer, C. S.; Taraszka, J. A.; Zientara, G. A.; Counterman, A. E.; Clemmer, D. E. Collision-Induced Dissociation of Mobility-Separated Ions Using an Orifice-Skimmer Cone at the Back of a Drift Tube. *Anal. Chem.* **2001,** *73,* 3549–3555.
45. Hoaglund-Hyzer, C. S.; Lee, Y. J.; Counterman, A. E.; Clemmer, D. E. Coupling Ion Mobility Separations, Collisional Activation Techniques, and Multiple Stages of MS for Analysis of Complex Peptide Mixtures. *Anal. Chem.* **2002,** *74,* 992–1006.
46. Ervin, K. M.; Armentrout, P. B. Translational Energy Dependence of $Ar^+ + XY \rightarrow ArX^+ + Y$ (XY = H_2, D_2, HD) from Thermal to 30 eV cm. *J. Chem. Phys.* **1985,** *83,* 166–189.
47. Schultz, R. H.; Armentrout, P. B. Reactions of N_4^+ with Rare Gases from Thermal to 10 eV c.m.: Collision-Induced Dissociation, Charge Transfer, and Ligand Exchange. *Int. J. Mass Spectrom. Ion Processes* **1991,** *107,* 29–48.
48. MATLAB; version 5.0.0.4073; The MathWorks Inc.; 1996.